Stability and Time-Delay Effect of Rainfall-induced Landslide Considering Air Entrapment

Shixin Zhang
Chongqing Three Gorges University
Li Li (lily6636694@163.com)
Chongqing Three Gorges University
Dongsheng Zhao
Chongqing Three Gorges University
Bo Ni
Chongqing Three Gorges University
Yue Qiang
Chongqing Three Gorges University
Zhou Zheng
Chongqing Three Gorges University

Research Letter

Keywords: rainfall-induced landslides, infinite slope, Green-Ampt infiltration model, air entrapment, hydraulic hysteresis

Posted Date: June 10th, 2021

DOI: https://doi.org/10.21203/rs.3.rs-589661/v1

Stability and time-delay effect of rainfall-induced landslide considering air entrapment

Shixin Zhang[a], Li Li[a]*, Dongsheng Zhao[a], Bo Ni[a], Yue Qiang[a], Zhou Zheng[a]

a) School of Civil Engineering, Chongqing Three Gorges University, Chongqing 404100, China

*Corresponding author

Email: lily66366943@163.com (L. Li)

Submitted on June 3, 2021

Abstract

Rainfall-induced landslide is a typical geological disaster in the Three Gorges reservoir area. The air entrapment in the pores of soils has a hindrance to the infiltration of the slope. It is mainly reflected in the hydraulic hysteresis after rainfall and the decrease of the slope anti-sliding force. A method considered the air entrapment of the closed gas in soil particles' pores is developed to study the time-delay effect and slope stability under the rainfall process. The Green-Ampt infiltration model is used to obtain the explicit analytical solution of the slope infiltration considering air entrapment. Moreover, the relationship between the safety factor, the rainfall duration, and the depth of the wetting front under the three rainfall conditions (q_{rain}=12, 26, 51 mm/h) is discussed. The results show that the air entrapment causes a significant time-delay effect of the landslide, and the hydraulic hysteresis is the strongest under the condition of heavy rainfall (q_{rain}= 51mm/h). The time-delay effect lasts longer than low rainfall and heavy rainfall when the rainfall intensity (q_{rain}= 26 mm/h) is slightly greater than saturated hydraulic conductivity K_s. Parameter analysis shows that when air entrapment is considered, the smaller the slope angle and the effective internal friction angle, the more significant the air entrapment has on the slope stability; the smaller the effective cohesion, the longer the air resistance lasts. Finally, the application of the Bay Area landslide is consistent with the actual state of the landslide.

Keywords: rainfall-induced landslides; infinite slope; Green-Ampt infiltration model; air entrapment; hydraulic hysteresis

1 Introduction

Rainfall-induced landslides are the most common type of landslide disaster (Higgitt et al. 2014; Li et al. 2020a; 2020b). The rainfall-induced landslide caused devastating disasters to mountain residents, such as many economic losses and casualties (Saito et al. 2017; Fustos et al. 2020; Yang et al. 2020).

The Green-Ampt (GA) infiltration model is similar to Darcy's law (Huo et al. 2020), so the model has a clear physical meaning and good scalability. Since it was proposed, it has been widely used in infiltration research. Many studies have made various amendments and supplements on the application scope and conditions of the GA model, such as determining hydraulic parameters, the approximate solution of the theory, and the error analysis. The modified GA infiltration model was applied to the infiltration of stable rainfall conditions (Mein and Larson 1973), one of the widely recognized modified GA models. The recommended extension model is also applied in this paper. It is worth noting that the GA infiltration model in slope infiltration needs to overcome the defect which is not suitable for slope. Therefore, an improved GA model suitable for slope rainfall infiltration was proposed (Chen and Young 2006), and the sensitivity analysis of geometric parameters was carried out. The optimal parameters of the GA model for the sand, sandy clay, and clay under the rainfall were obtained by solving the objective function of the GA optimization model and Richards' equation, which provided an essential reference for the application of the GA infiltration model in slopes (Chen et al. 2015). In general, the GA model is used with the infinite slope model. The application range of the improved method has been extended to landslides all over the world (e.g.,

52 Muntohar and Liao 2009, 2010; Zhang et al. 2017; Wu et al. 2018). The rainfall threshold is
53 used as one of the indicators of rainfall-induced landslides, and it is also a standard tool for
54 expressing the time portion of landslide hazard analysis (Martinović et al. 2018). Therefore, the
55 saturated hydraulic conductivity is usually used as the critical rainfall intensity threshold for the
56 ponding water on the slope. In this paper, three rainfall intensity conditions are designed to
57 study the influence of air entrapment on the stability of infinite slopes during rainfall.

58 The rainfall infiltration process and the slope failure are not entirely synchronized for the
59 rainfall-induced landslide. Compared with rainfall, landslide hazards often have hysteresis and
60 have a noticeable time-delay effect. The time-delay effect is mainly caused by the air
61 entrapment during the rainfall process (Lu and Likos 2006; Lu et al. 2013; Chen et al. 2015).
62 The effect of air pressure in the soil on the infiltration when the pores are closed was verified
63 by Wang et al. (1997, 1998) through laboratory seepage tests. Test results pointed out that when
64 the air overcomes the critical air pressure and breaks through the saturated soil layer and escapes
65 the atmosphere, the pore air pressure of the unsaturated soil layer decreases. Unfortunately,
66 Wang's method is mainly used in agricultural irrigation (Vereecken et al. 2019; Gonçalves et
67 al. 2020). A laboratory test suitable for the Masa sandy loam soil from weathered granite rock
68 and a TUAT light clay and soils from volcanic ash considering the influence of air entrapment
69 on hydraulic conductivity was performed (Sakaguchi et al. 2005). Exhausted the air between
70 pores in a vacuum environment, and then immerse in the water again to trap the air. The
71 hydraulic conductivity measured by the falling head method decreases as the air content
72 increases. An approach to combine the generalized stress framework with the suction stress

retention and the suction stress characteristic curve was proposed (Lu and Godt 2008; Chen et al. 2017). The modified method indicated that it is necessary to consider the hydraulic hysteresis caused by air entrapment in rainfall-induced landslides. Otherwise, the failure possibility of the infinite slope will often be underestimated. The hydraulic hysteresis of the wetting front is verified by field and laboratory experiments (Ebel et al. 2018), and the difference in soil between dry and wet conditions is critical for rainfall-induced landslides.

The existed method does not quantify the effect of air entrapment in the strength failure criteria. Therefore, the objective of this paper is to develop a novel method based on Wang's air entrapment theory and the infinite slope model to simulate the infiltration in slopes and analyze the stability of rainfall-induced landslides. The rest of this paper is organized as follows:

Section 2 introduced the improved GA model considering the air entrapment and the stability analysis of an infinite slope. The infiltration stage is divided into the unsaturated infiltration stage before ponding water and air entrapment infiltration after ponding water. In Section 3, verification and parameter analysis of the proposed method were carried out through an infinite slope example. The proposed method was applied to a landslide located in Alameda County, California, in Section 4. Finally, the conclusions were drawn in Section 5.

2 Method

2.1 Assumptions

Rainfall-induced landslides have been an essential issue that geotechnical engineers have been paying attention to for a long time in geological disasters. However, the actual slope is often complicated. Therefore, in order to facilitate the solution, the infinite slope is usually used

94 as the study object.

95 There is a prominent wetting front in the slope in the rainfall infiltration. The known
96 conditions parameters are: the rainfall intensity q_{rain}; saturated hydraulic conductivity K_s; soil
97 suction ψ_f; slope angle α; atmospheric pressure P_0. And soil mechanical parameters are: the
98 saturated unit weight γ_s, effective cohesion c'; effective internal friction φ'; saturated moisture
99 content θ_s; initial moisture content θ_i.

100 Some reasonable assumptions about the infiltration model were used in previous studies,
101 and their rationality had proved (Chen and Young 2006; Huang et al. 2008; Cevasco et al. 2014;
102 Dolojan et al. 2021; Zhang et al. 2021). Therefore, before deriving the model, the following
103 assumptions are made in this paper:

104 (1) The rainfall is uniform, that is, the total amount of the rainfall is constant;

105 (2) When $q_{rain}>K_s$, the soil above the wetting front is saturated. Unsaturated soil with initial
106 moisture content below the wetting front. In contrast, when $q_{rain}>K_s$, the soil is unsaturated.

107 (3) The bottom of the slope is regarded as impermeable bedrock, and the impact of
108 groundwater on infiltration is not considered.

109 (4) The modified GA model considering the air entrapment and proposed stability analysis
110 method is suitable for soil slopes or accumulative slopes.

111 **2.2 Non-ponding water stage**

112 At the beginning of rainfall, unsaturated soils absorb water. According to the GA model,
113 the rate of water infiltration q_{w1} in the slope determined by the rainfall intensity q_{arin} is:

114 $$q_{w1} = q_{rain} \cos\alpha \tag{1}$$

115 During the infiltration process, the air in the soil escapes freely from the slope surface as
116 the wetting front propagates downward. At this time, the pore air pressure in the saturated soil
117 layer is not compressed, so there is no air entrapment. Therefore, when the $q_{rain}<K_s$, the
118 traditional Green-Ampt infiltration model (del Vigo et al. 2021) can be used to obtain the
119 amount of infiltration:

120 $$F = \int_0^{z_w} [\theta_s - \theta_i] dy \tag{2}$$

121 where, F represents cumulative infiltration amount during rainfall; θ_s and θ_i represent the
122 saturated moisture content and the initial moisture content, respectively.

123 The differentiation of rainfall concerning time t is the rainfall intensity (or infiltration rate),
124 so the function of the depth of the wetting front and the rainfall intensity (or infiltration rate)
125 can be obtained:

126 $$\frac{dz_w}{dt} = \frac{q_{rain} \cos \alpha}{\theta_s - \theta_i} \tag{3}$$

127 In addition, a special infiltration situation which is no ponding water on the slope surface,
128 also needs to be considered. When $q_{rain}<K_s$, the soil in the slope is always unsaturated. Therefore,
129 it is necessary to solve the soil volumetric moisture content in the unsaturated state, and an
130 improved solution based on the Mein-Larson rainfall infiltration model was used to obtain the
131 volumetric water content by solving the pressure head above the wetting front (Almedeij and
132 Esen 2014). Van Genuchten (VG model) soil-water characteristic curve is usually used to
133 describe the unsaturated hydraulic characteristics of soil (van Genuchten 1980). The VG model
134 can be written:

$$\theta(h)=\begin{cases}\theta_r+\dfrac{\theta_s-\theta_r}{[1+(\alpha|h|)^n]^m}, h<0\\ \theta_s, h>0\end{cases} \tag{4}$$

where, $\theta(h)$ is the volumetric moisture content function; θ_r is the residual moisture content; h is the pressure water head; α and n are suggested parameters (in this paper, α=3.5 m^{-1} and n=1.5), and m=1-1/n.

The rainfall intensity q_{rain} in the unsaturated infiltration can be obtained:

$$q_{rain}=K_s\frac{\{1-(\alpha|h_w|)^{n-1}[1+(\alpha|h_w|)^n]^{-m}\}^2}{[1+(\alpha|h_w|)^n]^{m/2}} \tag{5}$$

where, h_w is the pressure water head when the moisture content reaches θ_w.

By solving Eq. (5), the volumetric moisture content when the pressure water head is h_w can be obtained. Then according to Eq. (2), the explicit expression of the infiltration depth z_w and rainfall duration when $q_{rain}<K_s$ is:

$$z_w=\frac{q_{rain}t}{\theta_w-\theta_i} \tag{6}$$

2.3 Ponding water stage

According to Darcy's law, the rate of water infiltration q_{w2} when ponding water on the slope surface is:

$$q_{w2}=K_s\frac{\psi_f+z_w\cos\alpha+h_0-h_f}{z_w} \tag{7}$$

where, K_s represents the saturated hydraulic conductivity; h_{af} represents the air pressure below the wetting front; ψ_f represents the suction.

When water is accumulated on the slope surface, the critical wetting front depth z_p is expressed as:

$$z_p = K_s \frac{\psi_f + h_0}{\cos\alpha(q_{rain} - K_s)} \tag{8}$$

For the vertical one-dimensional infiltration z_w-t of homogeneous soil, the formula can be written:

$$q_{w3} \cdot dt = dF = \Delta\theta \cdot dz_w \tag{9}$$

where, $\Delta\theta$=θ_s - θ_i; F is the cumulative infiltration volume; q_{w3} is the infiltration rate after ponding water.

Therefore, the critical time t_p can be obtained is:

$$t_p = K_s \frac{\Delta\theta(\psi_f - h_0)}{\cos^2\alpha q_{rain}(q_{rain} - K_s)} \tag{10}$$

Substituting Eq. (10) into Eq. (9), the differentiation of the slope wetting front depth to the rainfall duration can be obtained:

$$\frac{dz_w}{dt} = \begin{cases} \dfrac{q_{rain}\cos\alpha}{\Delta\theta}, t \le t_p \\ K_s \dfrac{\psi_f + \cos\alpha z_w + h_0 - h_{af}}{z_w \Delta\theta}, t \ge t_p \end{cases} \tag{11}$$

The analytical solution between the depth and duration of the wetting front is obtained by solving Eq. (11):

$$t = \begin{cases} \dfrac{z_w \Delta\theta}{q_{rain}\cos\alpha}, z_w \le z_p \\ t_p + A - B, z_w > z_p \end{cases} \tag{12}$$

where, A and B can be drawn:

$$\begin{cases} A = \dfrac{\Delta\theta\left(z_w\text{-}z_p\right)}{K_s\cos\alpha} \\ B = \dfrac{\Delta\theta(\psi_f + h_0 - h_{af}^{'})}{K_s\cos\alpha}\ln\left(\dfrac{\psi_f + z_w\cos\alpha + h_0 - h_{af}^{'}}{\psi_f + z_p\cos\alpha + h_0 - h_{af}^{'}}\right) \end{cases} \tag{12a}$$

In the ponding water infiltration stage, due to the existed ponding water on the slope surface, the porous air cannot escape from the slope surface during the downward movement of the wetting front. Therefore, the air is compressed in the pores of soils under the wetting front. When the air pressure in the pores exceeds the critical pressure, the air will break through the water pressure and escape. Since the conductivity of air in porous media is better than that of water, the pore pressure will decrease rapidly after the air escapes. The schematic diagram of air compression and escape process is shown in Fig. 1.

The air-breaking value H_b and the air-closing value H_c are suggested to be used to describe the pressure head h_{af} in the pore (Wang et al. 1997), and the H_b an H_c can be expressed as:

$$H_b = h_0 + z_w + h_{ab} \tag{13}$$

$$H_c = h_0 + z_w + h_{wb} \tag{14}$$

where, h_{ab} is the air-bubbling capillary pressure value; h_{wb} is the water-bubbling value.

H_b and H_c represent the maximum value that is about to break through the slope area and the minimum value of air pressure after the air escapes, respectively. In the air compression process, when the air pressure is maximum, an air-flow barrier will be formed. The infiltration rate $q_{w\min}$ in this state is 0 m/h. According to Eq. (7), the infiltration depth z_0 when the air pressure reaches the maximum value can be obtained:

$$z_0 = \left[\frac{1}{2}(h_b^2 + h_0^2 + h_{wb}^2 + B^2) + h_b h_0 + h_b h_{wb} + h_0 h_b + h_{wb} B + h_{0B} - h_b B\right]^{\frac{1}{2}} - \frac{1}{2}(h_b + h_0 + h_{wb} + B) + z_p \tag{15}$$

where, B is the depth of air-flow barrier below the soil surface, and it was measured by Wang et al (1997).

The infiltration time at the minimum infiltration rate (maximum pore pressure) is:

$$t_0 = \frac{z_0}{K_s} + t_p \tag{16}$$

After the air escapes, the pore pressure quickly drops to the minimum and the infiltration rate increases to a maximum. The maximum infiltration rate $q_{w\max}$ can be expressed as:

$$q_{w\max} = K_s \frac{h_{ab} - h_{wb}}{z_w} \tag{17}$$

Regarding the infiltration rate q_{wair} under air entrapment as a linear change, it can be drawn:

$$q_{wair} = \frac{q_{w\min} + q_{w\max}}{2} = \frac{K_s\left(h_{ab} - h_{wb}\right)}{2z_w} \tag{18}$$

When the air breaks through the ponding water, the infiltration duration t can be expressed as:

$$t = t_0 + \frac{z_w^2 - z_0^2}{K_e\left(h_{ab} - h_{wb}\right)} \tag{19}$$

where, K_e is the effective permeability coefficient, $K_e = z_0/t_0$.

$$z_w = [z_0^2 + K_e(h_{ab} - h_{wb})(t - t_0)]^{1/2} \tag{20}$$

In summary, three stages are mainly considered in the infiltration process: 1) non-ponding water stage. When $q_{rain} < K_s$, the unsaturated soil is considered in the infiltration. The Eq. (6) is used to solve the infiltration duration t; 2) early ponding water stage. The air entrapment tends to the maximum limit value. After the critical time t_p, the air entrapment is maximized after the time t_0, and then the air escapes from the slope surface. Eq. (12) is used to obtain the depth of the wetting front. 3) conventional ponding water stage. A linear function is used to describe the change of air entrapment in the conventional ponding water stage and Eqs. (19)-(20) is used to calculate the infiltration time and wetting front depth.

2.4 Safety factor of the infinite slope

For infinite slopes, the decrease of suction at the wetting front leads to a decrease in shear strength. The soil in the upper zone of the wetting front increases its unit weight due to the change in moisture content. Therefore, the critical slip surface is often the wetting front. According to the Mohr-Coulomb criterion and the shear strength theory of cohesive unsaturated soils (Duncan et al. 2014; Renani and Martin 2020):

$$FOS = \frac{(\sigma_n - u)\tan\varphi' + c'}{\tau} \tag{21}$$

where, σ_n is the normal stress at the bottom of the slope; τ is the sliding force; c' is the effective cohesion; φ' is the effective internal friction.

The normal stress σ_n and sliding force τ can be calculated according to the following formulas:

$$\sigma_n = \gamma_s z_w \cos^2\alpha + \gamma_w h_0 \cos^2\alpha \tag{22}$$

$$\tau = \gamma_s z_w \cos\alpha \sin\alpha \tag{23}$$

In an infinite slope, the normal force and shear force between the two sides of the soil slice are both 0. The weight of soil slice W above the wetting front should be calculated using saturated unit weight γ_s:

$$W = \gamma_s z_w \cos\alpha \tag{24}$$

After ponding water on the slope surface, the pressure on the slope surface G_w is:

$$G_w = \gamma_w h_0 \cos^2\alpha \tag{25}$$

During the downward movement of the wetting front, the pore air in the unsaturated soil layer below the wetting front is compressed. It can be seen from Fig. 1 that a water-air interface

is formed at the wetting front. The compressed pore air pressure supports the upper saturated soil layer and slows down the tendency of infiltration. The supporting force of the water at the wetting front can be expressed as:

$$P_a = \gamma_w h_{af}^{'} \cos^2 \alpha \tag{26}$$

where, $h_{af}^{'}$ is the average air pressure head, $h_{af}^{'}$=1/2(h_{ab}+h_{wb}).

When the air in the lower zone of the wetting front is restricted, Eq. (21) can be written as:

$$FOS = \frac{c' + (\sigma_n - P_a)\tan\varphi' + \gamma_w \psi_f \tan\varphi^b}{\tau} \tag{27}$$

Substituting Eqs. (22)-(26) into Eq. (27), the slope safety factor considering air entrapment can be obtained:

$$FOS = F_1 + F_2 + F_3 \tag{28}$$

where, $F_1 = \frac{c'}{\gamma_s z_w \cos\alpha \sin\alpha}$ □

$F_2 = \frac{(\gamma_s z_w - \gamma_w h_{af}^{'})\tan\varphi'}{\gamma_s z_w \tan\alpha}$ □

$F_3 = \frac{\gamma_w \psi_f \tan\varphi^b}{\gamma_s z_w \cos\alpha \sin\alpha}$

It can be drawn from Eq. (28) that the safety factor of the infinite slope considering the air entrapment during the infiltration process is mainly composed of three parts. The first part F_1 is mainly determined by the effective cohesion, the second part F_2 is mainly determined by the effective internal friction angle and the air entrapment, and the third part F_3 is mainly related to the suction of the wetting front. Substituting Eqs. (6), (12), (19) into Eq. (28) can get the analytic solution of the slope safety factor.

3 Infinite slope cases

The shallow infinite slope is used as the object of the calculation example. The detailed slope geometric parameters and mechanical parameters are shown in Table 1. The detailed hydrological parameters are shown in Table 2. In this paper, three rainfall conditions (α=40 °, φ'=36 °, c'=3 kPa) are designed based according to the Green-Ampt model. Condition 1 is rainfall intensity of 12 mm/h, simulating low rainfall; Condition 2 is the rainfall intensity of 26 mm/h, which is slightly larger than the saturated permeability coefficient of the soil; Condition 3 is the rainfall intensity of 51 mm/h, which simulates heavy rainfall and can reflect the time-delay effect. The infiltration process and slope stability analysis under three rainfall conditions to study the air entrapment were conducted. The calculation method based on the limit method proposed by Zhang et al. (2011) is used for the rainfall-induced slope without considering the air entrapment.

3.1 Hydraulic hysteresis caused by air entrapment

For the convenience of description, the five cases under the three conditions in this paper are recorded as Case 1 (q_{rain}=0.012 m/h), Case 2 (q_{rain}= 0.026 m/h with air entrapment), Case 3 (q_{rain}=0.026 m/h without air entrapment), Case 4 (q_{rain}=0.051 m/h with air entrapment), Case 5 (q_{rain}=0.051 m/h without air entrapment).

The change curves of the depth of the wetting front with the rainfall duration under the three rainfall conditions are shown in Fig. 2. The rainfall intensity q_{rain} of Condition 1 (Case 1) is 12 mm/h, which is less than the saturated hydraulic conductivity K_s, so there will be no air entrapment in Condition 1. It can be concluded from Fig. 2 that the wetting front of Condition 3 (Cases 4 and 5) moves down the fastest. When the depth of the wetting front is less than the

272 critical depth of the wetting front, the migration curve of the wetting front almost overlaps in
273 the two cases. This is because the rate of water infiltration is more significant in the early stage
274 of infiltration than the rainfall intensity. No water is formed on the slope surface, and the
275 rainwater is not affected by the air entrapment during the infiltration. When the rainfall duration
276 exceeds t_p, air entrapment needs to be considered. Evident hydraulic hysteresis appears when
277 considering the air entrapment in Condition 2 (Cases 2 and 3) and Condition 3 (Cases 4 and 5).
278 The time to reach a specific infiltration depth when the infiltration depth increases from 2 m to
279 3 m under Condition 2 (Cases 2 and 3) is given in Table 3. The Δt at the wetting front is 2 m,
280 2.25 m, 2.50 m, 2.75 m, and 3.00 m in the proposed model and the traditional infiltration model
281 are 0.45 h, 29.27 h, 63.45 h, 101.69 h, and 143.99 h, respectively. It can be seen from Table 3
282 that the air entrapment has a significant hydraulic hysteresis on the infiltration process.
283 However, in Condition 2, the hydraulic hysteresis in the infiltration process is more significant
284 than Condition 3. When the rainfall intensity is slightly larger than the saturated hydraulic
285 conductivity, the air entrapment will last longer. In rainfall-induced landslides, short-duration,
286 high-intensity rainfall is often more likely to cause shallow landslides (Larsen and Simon 1993).
287 Therefore, attention should be paid to the impact of short-duration, high-intensity rainfall on
288 landslides.

289 Fig. 3 shows the change curves of safety factors and rainfall duration in five cases. It can
290 be seen from Fig. 3 that under Case 4 and Case 5 (heavy-rainfall), the decline rate of the slope
291 safety factor is significantly greater than that under Case 1 (low-intensity rainfall) and Case 2
292 and Case 3 (moderate-intensity rainfall). Moreover, there are apparent time-delay effects in

293 Case 4 and Case 5. When the safety factor is reduced to the same, it takes significantly longer
294 to consider the slope of air entrapment. Furthermore, with the progress of the rainfall process,
295 this time is still increasing. It is worth noting that when the safety factor of the slope without
296 considering the air entrapment is lower than 1.0, the safety factor of the slope considering the
297 air entrapment is still greater than 1.0. This time difference is critical for disaster decision-
298 making.

299 **3.2 Parametric analysis**

300 The rainfall intensity has a significant effect on the stability of soil slopes. In Condition 3,
301 the infinite slope stability during the rainfall process is analyzed in this paper. Furthermore, the
302 impacts of different slope angles, effective cohesion, and effective internal friction angle on the
303 safety factor are compared. In Condition 3, the critical infiltration depth is small when the air
304 entrapment is exerted due to the greater rainfall intensity. In addition, the critical wetting front
305 depth is 0.07 m, so it is not additionally marked in Fig. 3. It can be seen from Fig. 4 that when
306 the depth of the wetting front exceeds 1.99 m and 2.13 m, respectively, the safety factors of
307 Case 3 and Case 4 are lower than 1.0, and they are in an instability state. Furthermore, Case 5
308 is in an unstable state on the slope, and its safety factor has fallen faster than Case 4. This is
309 caused by the gradual weakening of the air entrapment in the later stage of infiltration.

310 (a) Slope angle

311 Under Condition 3, the effect of different slope angles (α=20°, 40°, and 60°) on the safety
312 factor is studied. It can be seen from Fig. 5 that the slope angle has a significant impact on the
313 safety factor. With the increase of the slope angle, the decrease of the safety factor is pronounced.

The smaller the slope angle, the more obvious the hysteresis in the early stage of infiltration. It is worth noting that as the slope angle increases, the hysteresis caused by air entrapment gradually weakens. This is because the larger slope leads to a faster infiltration process.

(b) Effective cohesion

Fig. 6 shows the effect of different effective cohesion (c'=3, 8, 13 kPa) on the safety factor in Condition 3. Other parameters are consistent with those given in Section 3 and Table 1 and 2. It can be seen from Fig. 6 that the effective cohesion also has a significant impact on the safety factor. Considering the air entrapment in the early stage of infiltration will obtain a lower safety factor. At the same time, it will also have an obvious hydraulic hysteresis. By comparing Fig. 5 and Fig. 6, it can be found that the effective cohesion is more sensitive to the safety factor in the early stage of infiltration than the slope angle. This is because as the saturation unit weight of the upper soil layer increases, the role played by the effective cohesion gradually decreases.

(c) Effective internal friction angel

Fig. 7 shows the effect of different effective internal friction angles (φ'=24°, 36°, 48°) on the safety factor in Condition 3. Other parameters are consistent with those given in Section 3 and Table 1 and 2. It can be seen from Fig. 7 that as the infiltration duration increases, the effect of the internal friction angle on the safety factor becomes more evident. The safety factor of slopes with low internal friction angles decreases with the increase of the depth of the wetting front slightly faster than slopes with high internal friction angles.

4 Discussion

In this section, an actual landslide located in Alameda County, California (Fig. 8) is used

335 to verify the results of this paper and compare with the method proposed by Chen et al. (2017).
336 The detailed calculation parameters can be seen in Table 4. The Bay Area landslide is covered
337 by the silt of approximately 1 m, derived from the weathering products of the underlying
338 sandstone bedrock.

339 It can be seen from Table 5 that the proposed method is consistent with the actual state.
340 Table 5 shows the corresponding relationship between the infiltration depth and the safety factor
341 in the colluvial soil layer. Overall, the Bay Area landslide is still in a stable state. However,
342 when the wetting front depth is 0.8 m, the landslide is in an under-stable state. This result is
343 also consistent with the current state of the landslide (Chen et al. 2017). At the same time, the
344 safety factor calculated by the proposed method is lower than Chen's method. The normal stress
345 at the bottom of the soil slice and the anti-sliding force is reduced by the air entrapment. When
346 the rainfall intensity is much greater than the saturated hydraulic conductivity of the soil, the
347 air entrapment has a significant impact on slope stability. This is due to the rapid development
348 of the rainfall infiltration process, and the air below the saturated soil layer is rapidly
349 compressed, resulting in a significant hydraulic hysteresis in a short time. At the beginning of
350 rainfall, the air entrapment is sufficient to affect the normal stress σ_n at the wetting front. As the
351 infiltration progresses, the air entrapment caused by the air between the soil particles undergoes
352 multiple compressed-escaped to a significant attenuation, and the impact on the slope stability
353 is gradually weak. Therefore, it is suggested that Bay Area landslide should strengthen the
354 supervision of the landslide when the rainfall intensity q_{rain} is 2.52×10^{-7} m/s.

355 ## 5 Conclusions

In this paper, an analytic solution of rainfall-induced landslide considering air entrapment is proposed by combing the Green-Ampt model and the unsaturated soil shear strength criterion. Furthermore, the rainfall-induced landslides stability and time-delay effect caused by hydraulic hysteresis are also studied. In summary, the following conclusions can be drawn:

1) According to the analytical expression form, the analytical solution of the safety factor of rainfall-induced landslides considering air entrapment is mainly composed of three parts. Therefore, the factors affecting the slope stability under the rainfall can be summarized as soil mechanical parameters, air entrapment, and suction in unsaturated soil.

2) Considering the air entrapment on the infiltration process, the time to reach the same depth of the wetting front is significantly later than without considering the air entrapment. Therefore, the time-delay effect of air entrapment should not be ignored in the slope stability analysis. As a result, the slope safety factor is postponed after reaching the dangerous point, providing valuable time for disaster prevention and mitigation.

3) For external factors, rainfall intensity determines the influence of air entrapment on slope stability. The air entrapment under heavy rainfall causes the normal stress at the wetting front to decrease rapidly at the beginning of the rainfall, and the safety factor of the slope decreases significantly. Whereby, the hydraulic hysteresis is the most evident. For rainfall intensity slightly greater than the saturated hydraulic conductivity soil, the air entrapment lasts longer. However, the impact on slope stability is lower than that of heavy rainfall.

Acknowledgements

This work was supported by the Scientific and Technological Research Program of Chongqing Municipal Education Commission (Grant No. KJQN201901239, KJQN202001218,

KJQN202001219), General program of Chongqing Natural Science Foundation (Grant No. cstc2019jcyj-mscm1865).

Data availability statement

All data generated or analyzed during this study are included within the article.

Conflicts of interest

The authors declare that they have no conflict of interest.

References

Almedeij, J., & Esen, I. I. (2014). Modified Green-Ampt infiltration model for steady rainfall. Journal of Hydrologic Engineering, 19(9), 04014011.

Chen, L., Xiang, L., Young, M. H., Yin, J., Yu, Z., & van Genuchten, M. T. (2015). Optimal parameters for the Green-Ampt infiltration model under rainfall conditions. Journal of Hydrology and Hydromechanics, 63(2), 93-101.

Chen, L., & Young, M. H. (2006). Green‐Ampt infiltration model for sloping surfaces. Water resources research, 42(7).

Chen, P., Mirus, B., Lu, N., & Godt, J. W. (2017). Effect of hydraulic hysteresis on stability of infinite slopes under steady infiltration. Journal of Geotechnical and Geoenvironmental Engineering, 143(9), 04017041.

Chen, P., Wei, C., & Ma, T. (2015). Analytical model of soil-water characteristics considering the effect of air entrapment. International Journal of Geomechanics, 15(6), 04014102.

Cevasco, A., Pepe, G., & Brandolini, P. (2014). The influences of geological and land use settings on shallow landslides triggered by an intense rainfall event in a coastal terraced environment. Bulletin of Engineering Geology and the Environment, 73(3), 859-875.

del Vigo, Á., Zubelzu, S., & Juana, L. (2021). Infiltration models and soil characterisation for hemispherical and disc sources based on Green-Ampt assumptions. Journal of Hydrology, 595, 125966.

Dolojan, N. L. J., Moriguchi, S., Hashimoto, M., & Terada, K. (2021). Mapping method of rainfall-induced landslide hazards by infiltration and slope stability analysis. Landslides, 1-19.

Duncan, J. M., Wright, S. G., & Brandon, T. L. (2014). Soil strength and slope stability. John Wiley & Sons.

Ebel, B. A., Godt, J. W., Lu, N., Coe, J. A., Smith, J. B., & Baum, R. L. (2018). Field and Laboratory Hydraulic Characterization of Landslide‐Prone Soils in the Oregon Coast Range and Implications for Hydrologic Simulation. Vadose Zone Journal, 17(1), 1-15.

Fustos, I., Abarca-del-Rio, R., Moreno-Yaeger, P., & Somos-Valenzuela, M. (2020). Rainfall-Induced Landslides forecast using local precipitation and global climate indexes. Natural Hazards, 102(1), 115-131.

Gonçalves, R. D., Teramoto, E. H., Engelbrecht, B. Z., Alfaro Soto, M. A., Chang, H. K., & van Genuchten, M. T. (2020). Quasi‐Saturated Layer: Implications for Estimating Recharge and Groundwater Modeling. Groundwater, 58(3), 432-440.

Higgitt, D. L., Zhang, X., Liu, W., Tang, Q., He, X., & Ferrant, S. (2014). Giant palaeo-landslide dammed the Yangtze river. Geoscience Letters, 1(1), 1-7.

Huang, C. C., Lo, C. L., Jang, J. S., & Hwu, L. K. (2008). Internal soil moisture response to rainfall-induced slope failures and debris discharge. Engineering Geology, 101(3-4), 134-

145.

Huo, W., Li, Z., Zhang, K., Wang, J., & Yao, C. (2020). GA-PIC: An improved Green-Ampt rainfall-runoff model with a physically based infiltration distribution curve for semi-arid basins. Journal of Hydrology, 586, 124900.

Larsen, M. C., & Simon, A. (1993). A rainfall intensity-duration threshold for landslides in a humid-tropical environment, Puerto Rico. Geografiska Annaler: Series A, Physical Geography, 75(1-2), 13-23.

Li, S. H., Wu, L. Z., Chen, J. J., & Huang, R. Q. (2020a). Multiple data-driven approach for predicting landslide deformation. Landslides, 17(3), 709-718.

Li, S. H., Wu, L. Z., & Luo, X. H. (2020b). A novel method for locating the critical slip surface of a soil slope. Engineering Applications of Artificial Intelligence, 94, 103733.

Lu, N., & Godt, J. (2008). Infinite slope stability under steady unsaturated seepage conditions. Water Resources Research, 44(11).

Lu, N., & Likos, W. J. (2006). Suction stress characteristic curve for unsaturated soil. Journal of geotechnical and geoenvironmental engineering, 132(2), 131-142.

Lu, N., Kaya, M., Collins, B. D., & Godt, J. W. (2013). Hysteresis of unsaturated hydromechanical properties of a silty soil. Journal of Geotechnical and Geoenvironmental Engineering, 139(3), 507-510.

Martinović, K., Gavin, K., Reale, C., & Mangan, C. (2018). Rainfall thresholds as a landslide indicator for engineered slopes on the Irish Rail network. Geomorphology, 306, 40-50.

Mein, R. G., & Larson, C. L. (1973). Modeling infiltration during a steady rain. Water resources

research, 9(2), 384-394.

Muntohar, A. S., & Liao, H. J. (2009). Analysis of rainfall-induced infinite slope failure during typhoon using a hydrological–geotechnical model. Environmental geology, 56(6), 1145-1159.

Muntohar, A. S., & Liao, H. J. (2010). Rainfall infiltration: infinite slope model for landslides triggering by rainstorm. Natural hazards, 54(3), 967-984.

Renani, H. R., & Martin, C. D. (2020). Slope stability analysis using equivalent Mohr–Coulomb and Hoek–Brown criteria. Rock Mechanics and Rock Engineering, 53(1), 13-21.

Saito, H., Murakami, W., Daimaru, H., & Oguchi, T. (2017). Effect of forest clear-cutting on landslide occurrences: Analysis of rainfall thresholds at Mt. Ichifusa, Japan. Geomorphology, 276, 1-7.

Sakaguchi, A., Nishimura, T., & Kato, M. (2005). The effect of entrapped air on the quasi‐saturated soil hydraulic conductivity and comparison with the unsaturated hydraulic conductivity. Vadose Zone Journal, 4(1), 139-144.

Van Genuchten, M. T. (1980). A closed‐form equation for predicting the hydraulic conductivity of unsaturated soils. Soil science society of America journal, 44(5), 892-898.

Vereecken, H., Weihermüller, L., Assouline, S., Šimůnek, J., Verhoef, A., Herbst, M., ... & Xue, Y. (2019). Infiltration from the pedon to global grid scales: An overview and outlook for land surface modeling. Vadose Zone Journal, 18(1), 1-53.

Wang, Z., Feyen, J., Nielsen, D. R., & van Genuchten, M. T. (1997). Two‐phase flow infiltration equations accounting for air entrapment effects. Water Resources Research,

33(12), 2759-2767.

Wang, Z., Feyen, J., van Genuchten, M. T., & Nielsen, D. R. (1998). Air entrapment effects on infiltration rate and flow instability. Water Resources Research, 34(2), 213-222.

Wu, L. Z., Zhang, L. M., Zhou, Y., Xu, Q., Yu, B., Liu, G. G., & Bai, L. Y. (2018). Theoretical analysis and model test for rainfall-induced shallow landslides in the red-bed area of Sichuan. Bulletin of Engineering Geology and the Environment, 77(4), 1343-1353.

Yang, H., Yang, T., Zhang, S., Zhao, F., Hu, K., & Jiang, Y. (2020). Rainfall-induced landslides and debris flows in Mengdong Town, Yunnan Province, China. Landslides, 17(4), 931-941.

Zhang, S., Xu, Q., & Zhang, Q. (2017). Failure characteristics of gently inclined shallow landslides in Nanjiang, southwest of China. Engineering Geology, 217, 1-11.

Zhang, J., Zhu, D., & Zhang, S. (2020). Shallow slope stability evolution during rainwater infiltration considering soil cracking state. Computers and Geotechnics, 117, 103285.

Captions of Tables and Figures

Table 1 Soil physical parameters and rainfall conditions

Table 2 Hydraulic parameters

Table 3 Hydraulic hysteresis comparison

Table 4 Parameters for Bay Area landslide (Chen et al. 2017)

Table 5 The FOS of the colluvial soil layer

Fig. 1 Porous air compressed-escaped process

Fig. 2 Changes in the depth of the wetting front during rainfall

Fig. 3 Safety factor of 5 cases

Fig. 4 Safety factor and wet front depth change curve of Case 4 and Case 5

Fig. 5 Comparison of three different slope angles

Fig. 6 Comparison of three effective cohesions

Fig. 7 Comparison of three effective internal friction angles

Fig. 8 Scematic diagram of the field monitoring hillslope in Alameda County, California (Chen et al. 2017)

494 **Table 1** Soil physical parameters and rainfall conditions

γ_d /(kN·m^{-3})	γ_s /(kN·m^{-3})	φ^b /(°)	ψ_f /m	Condition 1 q_{rain}/(m·h^{-1})	Condition 2 q_{rain}/(m·h^{-1})	Condition 3 q_{rain}/(m·h^{-1})
16.5	21.7	6	0.06	0.012	0.026	0.051

495

496 **Table 2** Hydraulic parameters

γ_w (kN·m^{-3})	K_s (m·h^{-1})	θ_s %	θ_i %	θ_r %	h_{ab} /m	h_{wb} /m	h_{af}/m
9.8	0.0248	45	10	1.5	1.3	0.6	0.35

497

498 **Table 3** Hydraulic hysteresis comparison

z_w/m	Time required without air entrapment /h	Time required with air entrapment /h	Δt /h
2.00	35.25	35.70	0.45
2.05	36.14	40.99	4.89
2.10	37.04	47.75	10.71
2.15	37.93	54.67	16.74
2.20	38.83	61.75	22.92
2.25	39.73	69.00	29.27
2.30	40.62	76.41	35.79
2.35	41.52	83.98	42.46
2.40	42.42	91.71	49.29
2.45	43.32	99.61	56.29
2.50	44.22	107.67	63.45
2.55	45.12	115.89	70.77
2.60	46.02	124.28	78.26
2.65	46.92	132.83	85.91
2.70	47.82	141.54	93.72
2.75	48.72	150.41	101.69
2.80	49.62	159.45	109.83
2.85	50.53	168.65	118.12
2.90	51.43	178.01	126.58
2.95	52.33	187.54	135.21
3.00	53.23	197.22	143.99

499

500

501

502 **Table 4** Parameters for Bay Area landslide (Chen et al. 2017)

c' (kPa)	1.0
φ' (°)	20
φ^b (°)	6
α (°)	34
γ_w (kN/m^3)	9.81
γ_d (kN/m^3)	20.00
θ_s	0.50
α (°)	34
k_s (m/s)	2.59×10^{-8}
q_{rain} (m/s)	2.52×10^{-7}
h_{ab} (m)	0.54
h_{wb} (m)	0.23

503

504 **Table 5** The FOS of the colluvial soil layer

z_w	*FOS*	
	The proposed method	Chen's method
0.2	2.10	2.34
0.3	1.88	2.11
0.4	1.63	1.87
0.5	1.30	1.53
0.6	1.18	1.42
0.7	1.09	1.35
0.8	1.05	1.33
0.9	1.03	1.31
1.0	1.01	1.28

505

506

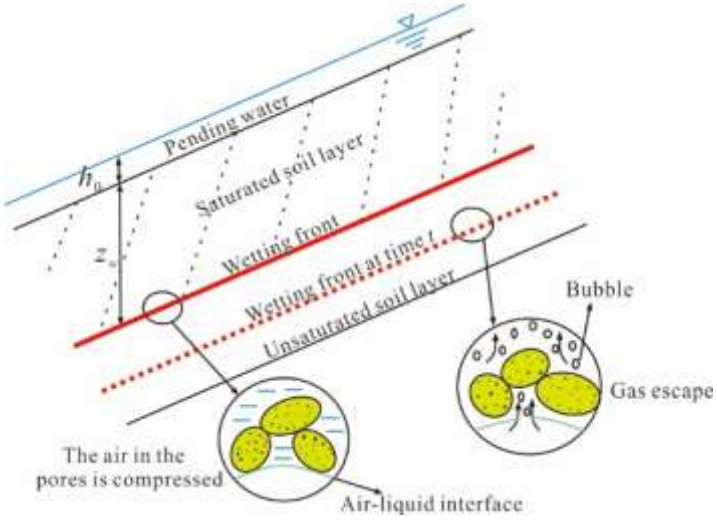

507

508 **Fig. 1** Porous air compressed-escaped process

509

510

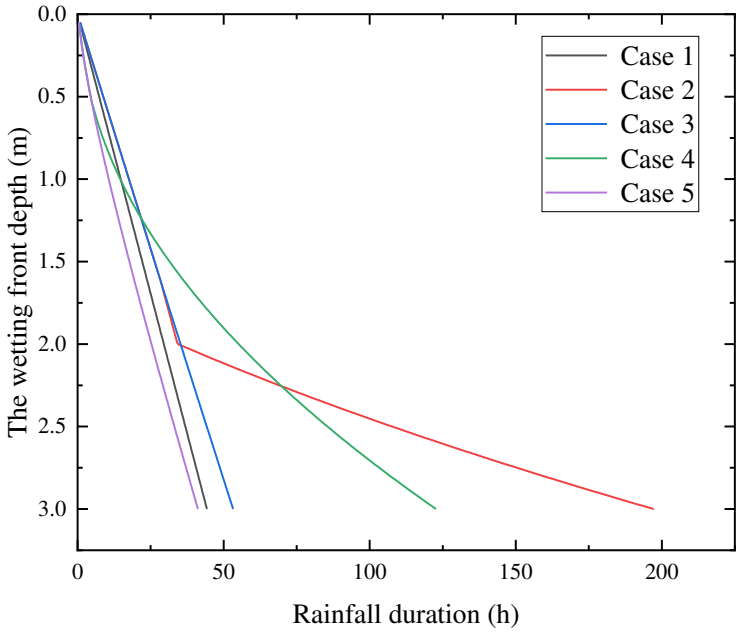

511

512 **Fig. 2** Changes in the depth of the wetting front during rainfall

513

514

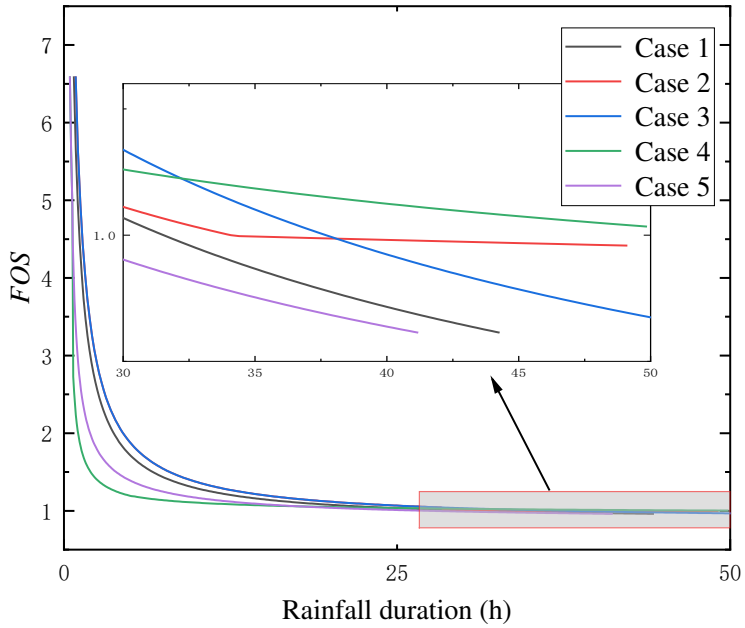

515

516 **Fig. 3** Safety factor of 5 cases

517

518

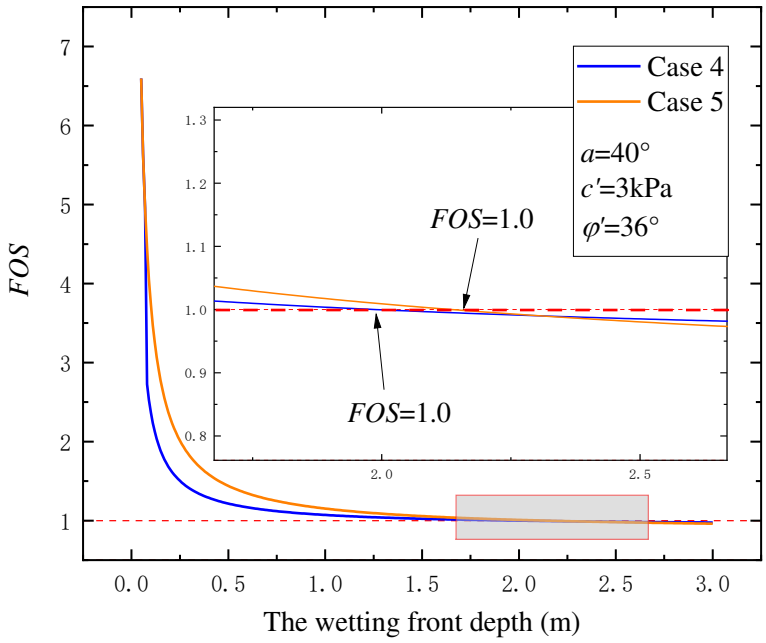

519

520 **Fig. 4** Safety factor and wet front depth change curve of Case 4 and Case 5

521

522

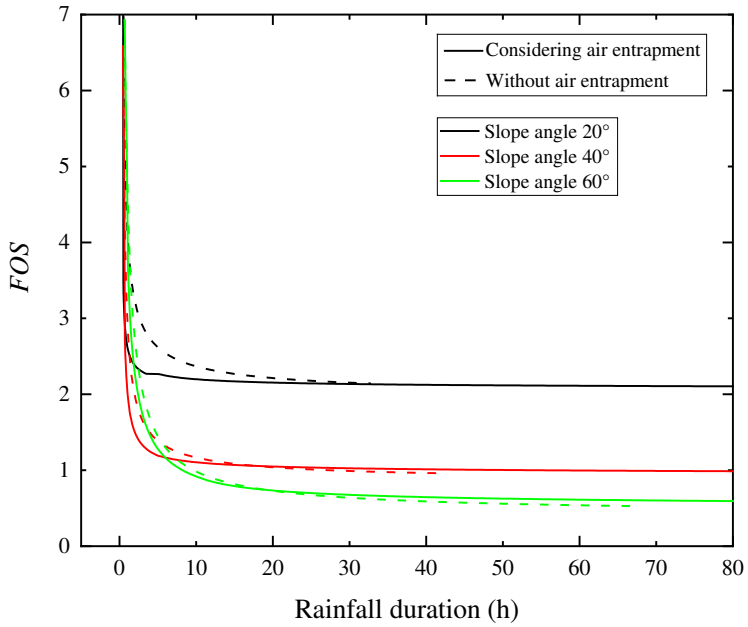

523

524 **Fig. 5** Comparison of three different slope angles

525

526

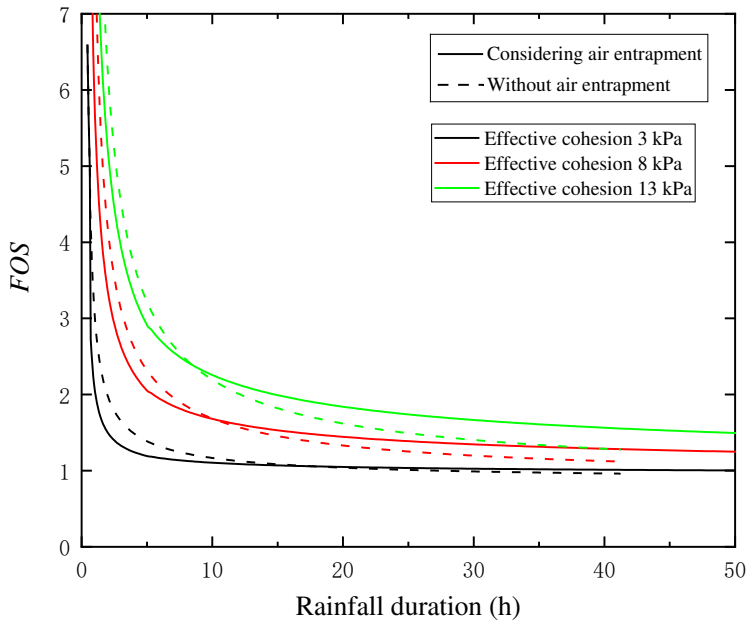

527

528 **Fig. 6** Comparison of three effective cohesions

529

530

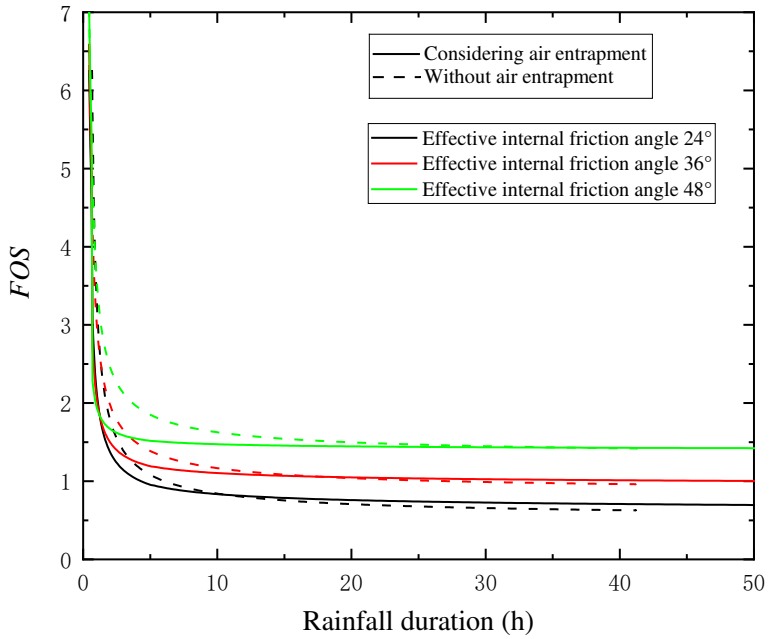

531

532 **Fig. 7** Comparison of three effective internal friction angles

533

534

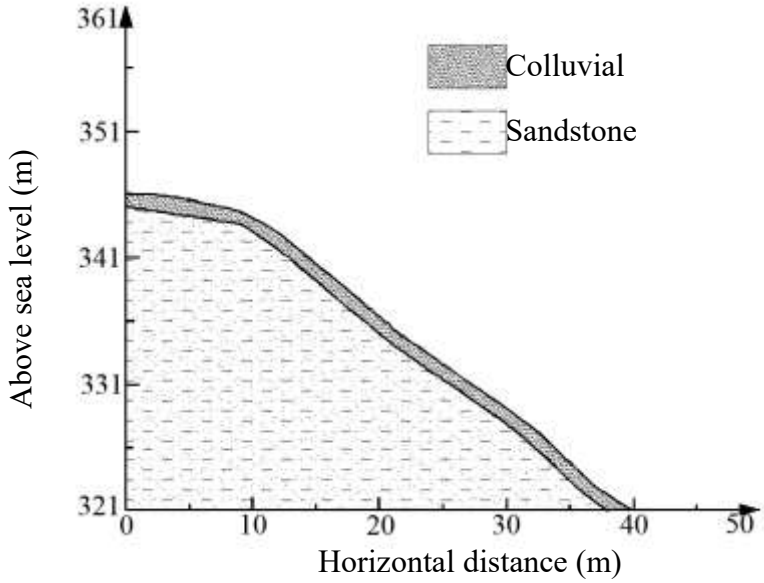

535

536 **Fig. 8** Scematic diagram of the field monitoring hillslope in Alameda County, California (Chen

537 et al. 2017)

538

Figures

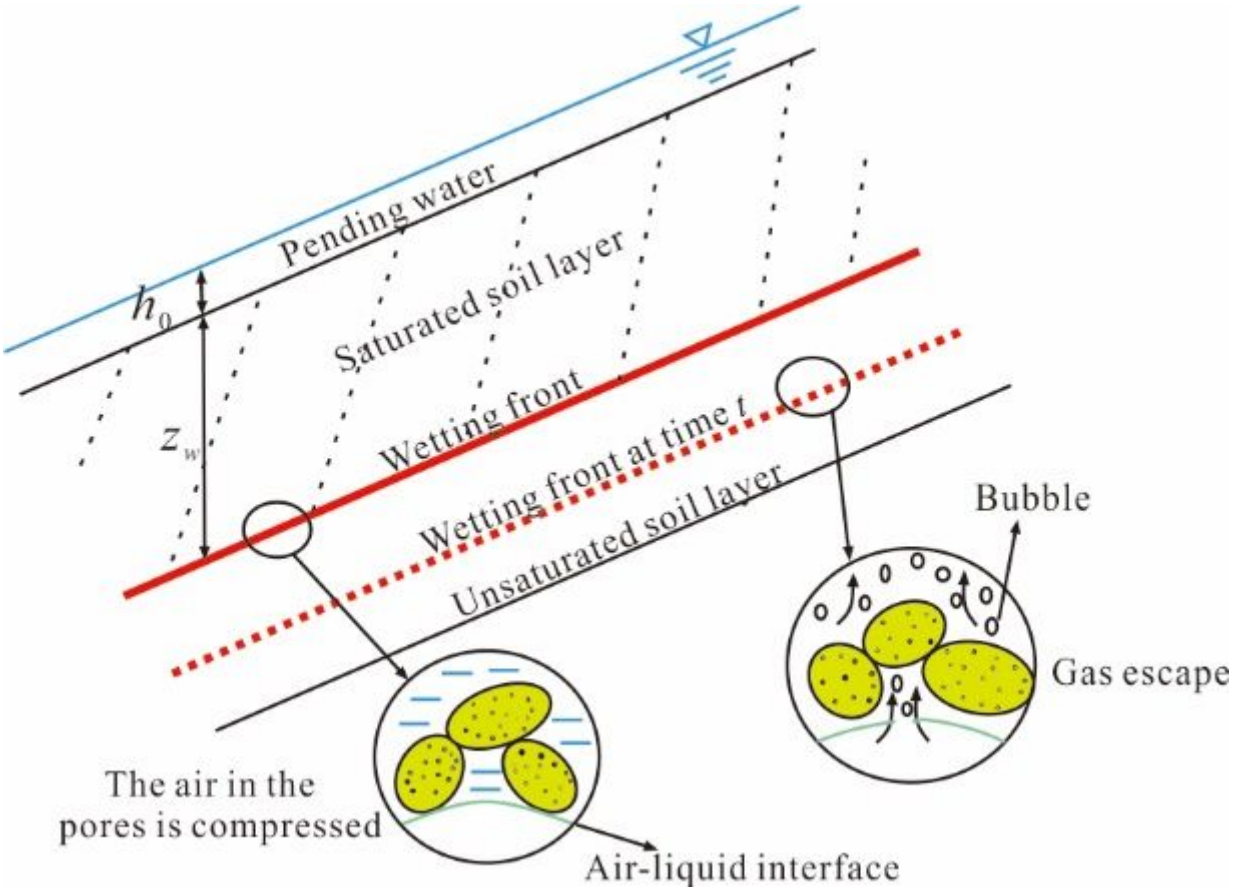

Figure 1

Porous air compressed-escaped process

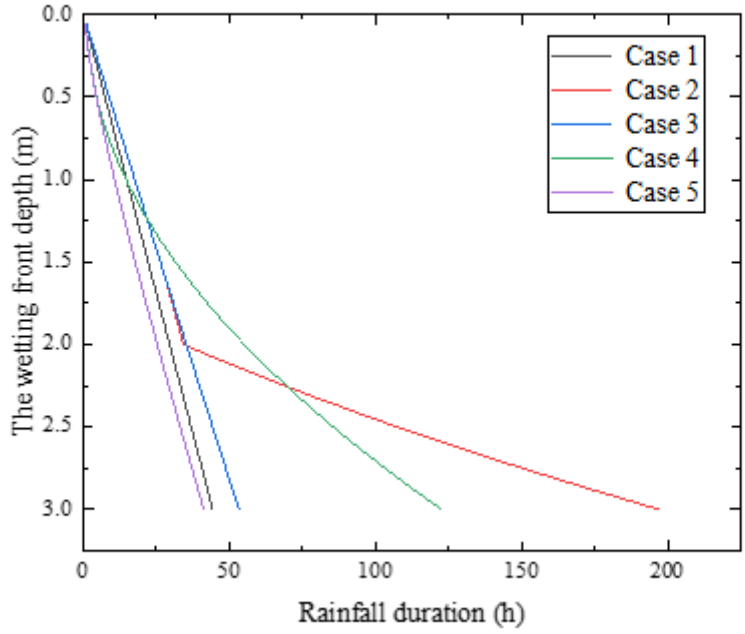

Figure 2

Changes in the depth of the wetting front during rainfall

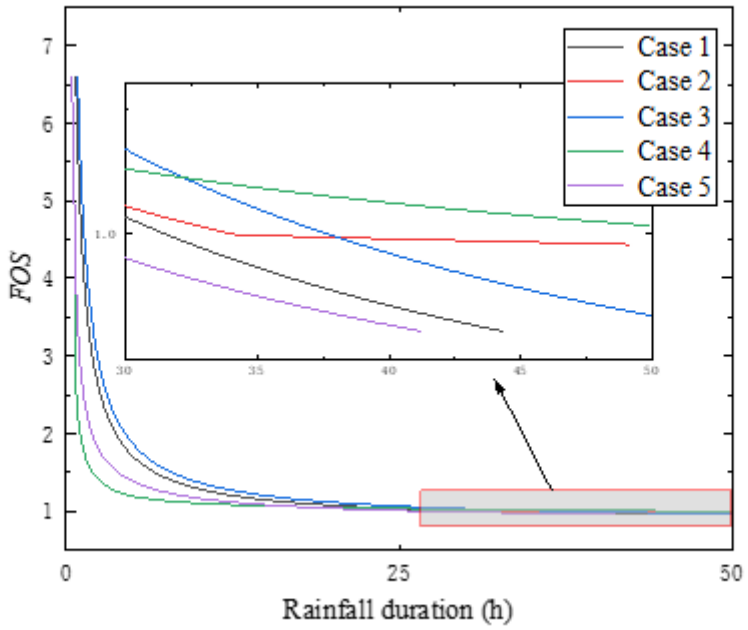

Figure 3

Safety factor of 5 cases

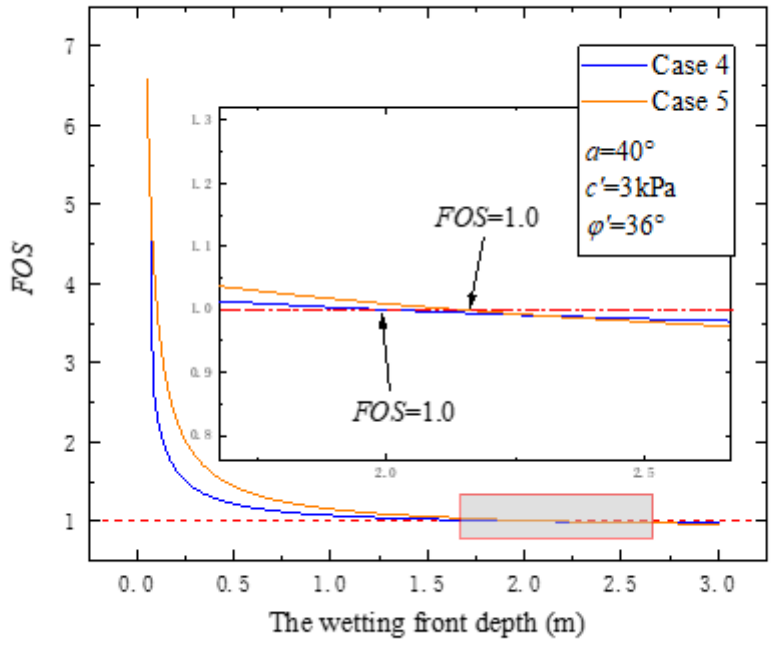

Figure 4

Safety factor and wet front depth change curve of Case 4 and Case 5

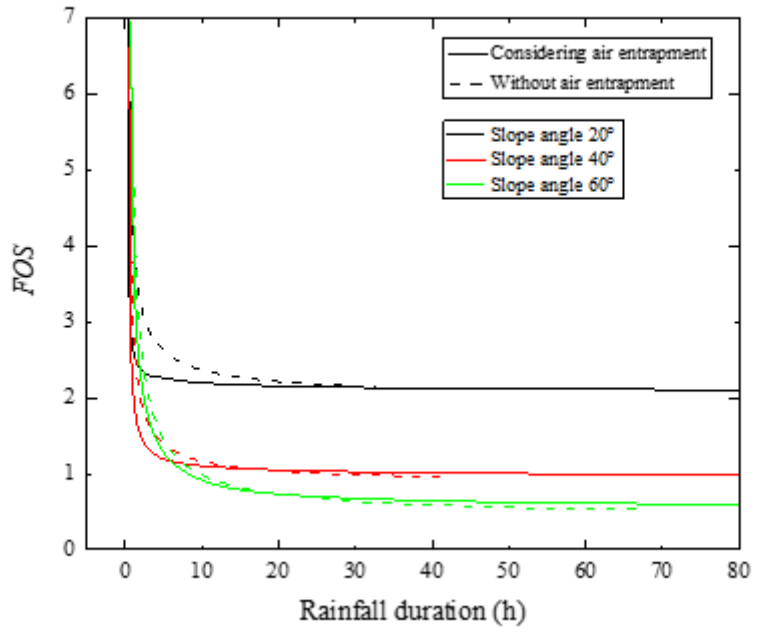

Figure 5

Comparison of three different slope angles

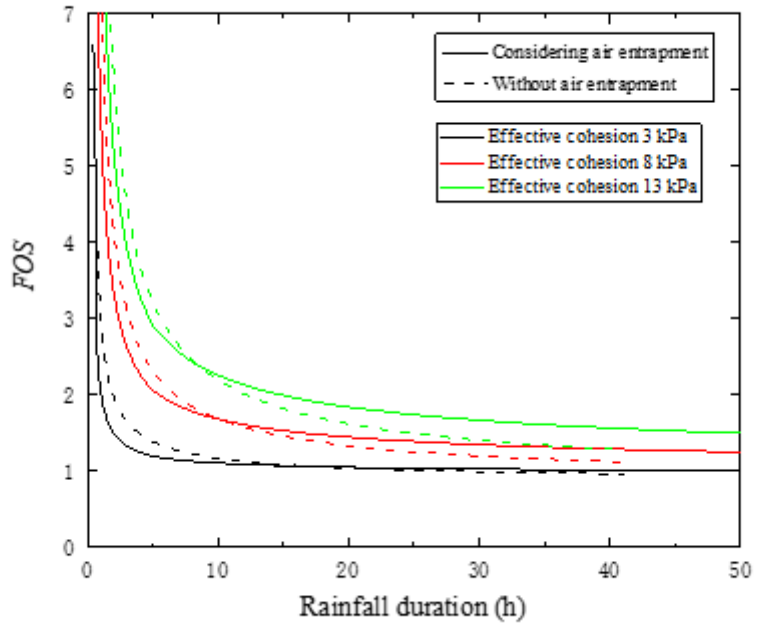

Figure 6

Comparison of three effective cohesions

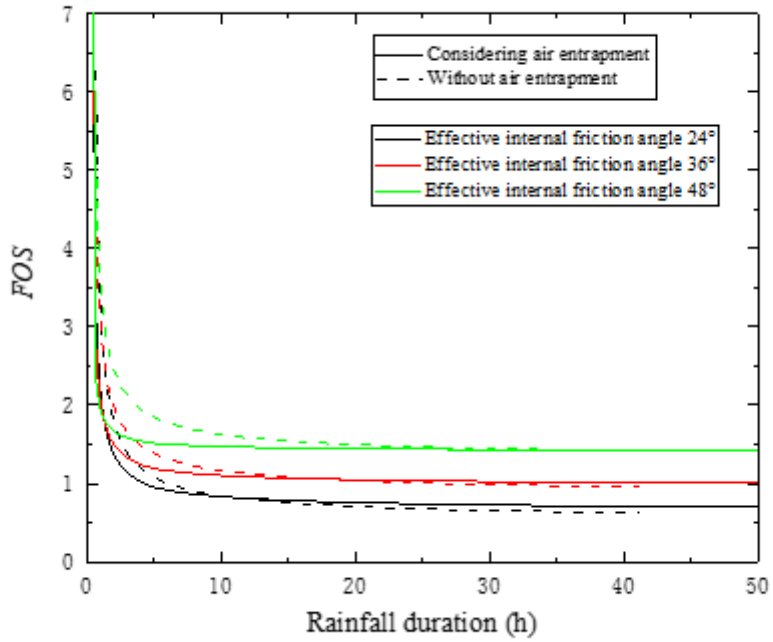

Figure 7

Comparison of three effective internal friction angles

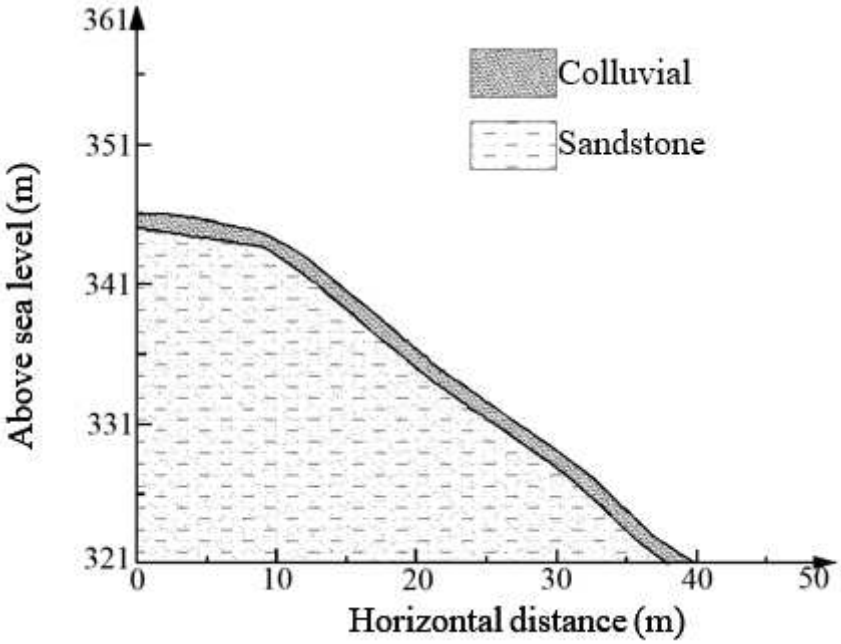

Figure 8

Scematic diagram of the field monitoring hillslope in Alameda County, California (Chen et al. 2017)